Available online at www.sciencedirect.com
SCIENCE DIRECT®
PERGAMON
Polyhedron 22 (2003) 1871–1876
POLYHEDRON
www.elsevier.com/locate/poly

Density functional studies of single molecule magnets

Jens Kortus [a,*], Mark R. Pederson [b], Tunna Baruah [c], N. Bernstein [b], C.S. Hellberg [b]

[a] Max-Planck-Institut für Festkörperforschung, Heisenbergstrasse 1, D-70569 Stuttgart, Germany
[b] Center for Computational Materials Science, Naval Research Laboratory, Washington, DC 20375-5000, USA
[c] Department of Physics, Georgetown University, Washington, DC 20057, USA

Received 6 October 2002; accepted 13 November 2002

Abstract

A method for the calculation of the second-order anisotropy parameters of single molecular magnets from the single particle orbitals is reviewed. We combine this method with density functional calculations to predict the magnetic anisotropy parameters of several single molecule magnets: Mn_{12}-acetate, Mn_{10}, Co_4, Fe_4, Cr_1 and V_{15}. Comparison with available experimental data shows that it is possible to predict these values quite accurately from density functional wavefunctions.

Keywords: Nanomagnets; Single-molecule magnets; Magnetic anisotropy; Density-functional calculations; Spin–orbit coupling

PACS numbers: 75.50.Xx; 71.24.+q

1. Introduction

Single-molecule magnets are being extensively studied because of their interesting properties such as quantum tunneling of magnetization [1,2] and quantum phase interference [3] on one hand and on the other hand to exploit these properties to build new data storage systems with significantly higher storage densities or in applications to quantum computing [4]. Below their blocking temperature, those molecules show magnetization hysteresis similar to bulk magnets. Unlike the bulk magnetization hysteresis, the hysteresis of the molecular magnets shows a step-like structure, which arises from the magnetization tunneling. These properties are governed by the magnetic anisotropy barrier of the system. This barrier has its origin in spin–orbit coupling [5]. In this article, we outline a method for the calculation of the anisotropy barrier by incorporating the spin–orbit coupling into a non-relativistic density-functional calculation and relying on second-order perturbation theory. We show that this treatment of spin–orbit coupling term is in effect exact to second-order and results in accurate prediction of the magnetic barriers.

At the time of the VIIth International Conference on Molecule-based Magnets in 2000 Miller suggested the question: 'How does one design materials with controlled zero-field splitting (D)?' was one of the 'unsolved mysteries' in the field of molecule-based magnets [6]. This work is an attempt to fill this gap and to understand the magnetic anisotropy parameters D and E from first-principles density-functional calculations. From the knowledge gained by these investigations we hope to derive information on how to control and modify these magnetic anisotropy parameters.

2. Theoretical details

Up to second-order, the anistropy Hamiltonian can in general be expressed as:

$$H = DS_z^2 + E(S_x^2 - S_y^2) \quad (1)$$

where D and E are known as axial and transverse anisotropy parameters. Recently, Pederson and Khanna have developed a method for accounting for second-order anisotropy energies [7]. This method relies on a

* Corresponding author. Tel.: +49-711-689-1664; fax: +49-711-689-1632.
E-mail address: j.kortus@fkf.mpg.de (J. Kortus).

0277-5387/03/$ - see front matter
doi:10.1016/S0277-5387(03)00160-8

simple albeit exact method for spin–orbit coupling and a second-order perturbative treatment of the spin Hamiltonian to determine the dependence of the total energy on spin projection. In this method, a Cartesian representation of the spin–orbit term is used which is exact and is also more convenient for multi-center systems. According to this method, the spin–orbit coupling term:

$$U(\mathbf{r},\ \mathbf{p},\ \mathbf{S}) = -\frac{1}{2c^2}\ \mathbf{S}\cdot\mathbf{p}\times\nabla\Phi(\mathbf{r}) \tag{2}$$

can be incorporated as given below. Using single-particle wavefunctions expressed in terms of a basis set:

$$\psi_{is}(\mathbf{r}) = \sum_{j,\sigma}\ C_{j\sigma}^{is} f_j(\mathbf{r})\chi_\sigma \tag{3}$$

where the $f_j(\mathbf{r})$ are the spatial functions and χ are spin functions, the matrix elements can be expressed as:

$$U_{j,\sigma,k,\sigma'} = \langle f_j\chi_\sigma|U(\mathbf{r},\ \mathbf{p},\ \mathbf{S})|f_k\chi_{\sigma'}\rangle \tag{4}$$

$$= -i\langle f_j|V_x|f_k\rangle\langle\chi_\sigma|S_x|\chi_{\sigma'}\rangle \tag{5}$$

where the operator V_x is defined as:

$$\langle f_j|V_x|f_k\rangle = \frac{1}{2c^2}\left(\left\langle\frac{df_j}{dz}\middle|\Phi\middle|\frac{df_k}{dy}\right\rangle - \left\langle\frac{df_j}{dy}\middle|\Phi\middle|\frac{df_k}{dz}\right\rangle\right) \tag{6}$$

In the above, $\Phi(\mathbf{r})$ is the Coulomb potential. Thus this treatment uses matrix elements of the Coulomb potential with partial derivatives of the basis functions, thereby avoiding the time consuming task of calculating the gradient of the Coulomb potential directly.

The implementation of the spin–orbit coupling has been tested on calculations of the energy level splittings of several free noble gas atoms because in that case one can compare with non spin polarized solutions of the Dirac equation [8]. Some results are shown in Table 1. Please note that the agreement improves significantly for the outer electronic shells, for which in general relativistic effects become less important. This is very important because a completely filled shell gives no contribution to the magnetic anisotropy energy. Only the states close to the Fermi level are important for the determination of the tunneling barriers.

Table 1
Spin–orbit splittings of energy levels (Δ_{SO} in Hartree) for Ar and Kr calculated with NRLMOL compared with results of a full relativistic numerical solution of the Dirac equation [8]

Δ_{SO}	Ar		Kr	
	NRLMOL	Dirac	NRLMOL	Dirac
2p	0.0796	0.0817	1.8731	1.9635
3p	0.0063	0.0066	0.2775	0.2897
3d	–	–	0.0471	0.0479

More important for the field of molecular magnetism is a direct comparison of the energy level splittings of transition metal ions to experimental data which includes the effect of spin–orbit splittings as well as the exchange splitting. We discuss two examples of Mn and Ru atoms in solids, where the electronic structure was probed directly by resonant X-ray scattering measurement. X-ray emission and absorption spectroscopies are powerful probes of the electronic structure of solids. Since dipole selection rules govern the transitions to or from a core level, it is actually the angular-momentum-resolved electronic density of states (DOS) that is measured. In the soft X-ray regime, one of the states is a localized, dispersionless core level. This allows for the interpretion of the measured spectra in terms of unoccupied states for absorption and occupied states for emission.

The first example compares directly the electronic structure of the molecule-based magnet $Mn[N(CN)_2]_2$ obtained from experiment and theory [9]. The Mn^{2+} ions are antiferromagnetically coupled at low temperatures and the local moments of the Mn atoms are reduced by about 10% as compared with an isolated ion due to partial covalent bonding. The splitting of the 2p-levels of Mn can be measured by the L-emission X-ray spectra of Mn. The experimental value of 11–12 eV is in good agreement with the calculated splitting of 10.3 eV. Also all other results obtained from Naval Research Laboratory Molecular Orbital Library (NRLMOL) are in good agreement with previous experiments [9].

Also for the case of a Ru atom in an octahedral oxygen environment which simulates $SrRuO_3$, a material of interest due to superconductivity, it was found that the calculated splittings of the core 2p levels are in excellent agreement with results of X-ray measurements within 1–3% of the total splitting [10].

From the good agreement to the numerical and experimental test cases we conclude that the implementation of the spin–orbit operator as described above works very reliably and is correct.

2.1. Magnetic anisotropy energy

In the absence of a magnetic field, the second-order perturbative change to the total energy of a system with arbitrary symmetry can be expressed as:

$$\Delta_2 = \sum_{\sigma\sigma'}\sum_{ij}\ M_{ij}^{\sigma\sigma'} S_i^{\sigma\sigma'} S_j^{\sigma'\sigma} \tag{7}$$

which is the generalization of Eq. (19) of Ref. [7]. In the above expression, σ sums over the spin degrees of freedom and i, j sums over all the coordinate labels, x, y, z, respectively. The matrix elements $S_i^{\sigma\sigma'} = \langle\chi^\sigma|S_i|\chi^{\sigma'}\rangle$ implicitly depend on the axis of quantiza-

tion. The matrix elements $M_{ij}^{\sigma\sigma'}$ are given by:

$$M_{ij}^{\sigma\sigma'} = -\sum_{kl} \frac{\langle\phi_{l\sigma}|V_i|\phi_{k\sigma'}\rangle\langle\phi_{k\sigma'}|V_j|\phi_{l\sigma}\rangle}{\varepsilon_{l\sigma} - \varepsilon_{k\sigma'}} \quad (8)$$

where $\phi_{l\sigma}$ and $\phi_{k\sigma'}$ are occupied and unoccupied states, respectively and ε's are the energy of the corresponding states.

A few relevant points about this method are that for electronic structure calculations which employ an analytical basis set such as Gaussians, it is easier to take the derivative of the basis functions rather than that of the Coulomb potential. The treatment uses the Cartesian formulation as given above which is exact and, therefore, accounts for all contributions from the nuclear and electronic potential which is a major part of the spin–other orbit effects. Further, although the spin–orbit coupling is not incorporated into the self-consistent cycle, the results are still quite accurate due to the fact that the first order perturbation to density due to the operator $-i\mathbf{V}\cdot\mathbf{S}$ vanishes. This follows from the fact that the first order corrections to orbitals are purely imaginary.

Our calculations include all single-determinantal two-electron interactions which have a classical origin due to the interaction of a moving spin 1/2 electron in a field of charge due to protons and electrons. It does not include any effects, which are related to multi-determinantal overlap. These effects may be small in the case that the metal-ion overlap is small as is the case for most single molecule magnets.

2.2. DFT implementation: NRLMOL

We combine the above treatment of the second-order zero-field spin Hamiltonian with the density functional based electronic structure calculations where the single-particle orbitals ϕ_i are the Kohn–Sham orbitals [11,12]. The non-relativistic density functional-based calculations are performed with the all-electron Gaussian-orbital based NRLMOL program [13–18], using the Perdew–Burke–Ernzerhof (PBE) generalized-gradient approximation for the exchange and correlation function [19]. NRLMOL combines large Gaussian orbital basis sets, numerically precise variational integration and an analytic solution of Poisson's equation in order to accurately determine the self-consistent potentials, secular matrix, total energies and Hellmann–Feynman–Pulay forces [20]. The exponents for the single Gaussians are fully optimized for DFT calculations [17]. The contraction coefficients for atomic orbitals are obtained by performing an SCF-LDA calculation on the spherical unpolarized atom where the total energy of the atom is converged to within 10 meV. The basis functions which do not correspond to atomic wavefunction are constructed from the longest range bare Gaussians in the basis set. All computationally intensive parts of the code are massively parallized which allows for the first-principle treatment of systems with 100–200 atoms within density-functional theory [18,21,22].

We present a few case studies using the above mentioned method. We would like to point out that it is necessary to get the correct spin-ordering of the system from the electronic structure calculation. Another pertinent point is the HOMO–LUMO gap of the system. From the Eq. 8, it is clear that the barrier will increase for systems with small gaps. Although, it appears that a large spin and a small gap will help in enhancing the barrier of the system, we find that it is a subtle interplay between several other effects that determines the barrier.

3. Application to single molecule magnets

In Table 1 we present the calculated D and E parameters for a few single molecule magnets and compare with the available experimental values. We show the actual molecular symbols in the table and refer to these molecules in the text by their transition metal core since it is these atoms which are responsible for their magnetic behavior. In all the cases presented here the spin ordering is in agreement with experiment. In all cases except Fe_4, the geometries were optimized until the forces on the atoms became negligible. The geometry optimizations were carried out at the all-electron level and to reduce computational costs, the symmetry of the molecule was exploited whenever possible.

The calculated D and E parameters for Mn_{12}, Mn_{10}, the ferric star Fe_4 and Cr-amide molecular magnets are in excellent agreement with experimental values. The single molecule magnets are in general characterized by a high spin ground-state. However, as can be seen from Table 2, a high spin state does not necessarily correlate with a high anisotropy barrier.

Some detailed discussion of our results will be given below.

3.1. Mn_{12}-acetate

The Mn_{12} molecule has S_4 symmetry and, therefore, the calculations were carried out using only 25 inequivalent atoms. Moreover, in Mn_{12}, the acetate units were replaced by formate groups (OOCH) so as to reduce the computational efforts while keeping the core of the molecule the same. This molecule has ferrimagnetic spin ordering with an inner core of Mn_4O_4 of minority spin atoms and an outer ring of Mn_8O_8 majority spin atoms. The inner-core Mn atoms have spin magnetic moment of -3 μ_B whereas the outer ones have 4 μ_B thus leading to a net magnetic moment of 20 μ_B.

Table 2
Comparison of the calculated and experimental magnetic anisotropy parameters for the single molecule magnets discussed in the text

Molecule	S	D (K)		E (K)		Type	References	
		Theory	Experimental	Theory	Experimental		Theory	Experimental
$Mn_{12}O_{12}(O_2CH)_{16}(H_2O)_4$	10	−0.56	−0.56	0	0	uniaxial	[7,22]	[23]
$[Mn_{10}O_4(2,2'\text{-biphenoxide})_4Br_{12}]^{4-}$	13	−0.06	−0.05	0	0	uniaxial	[24]	[25]
$Co_4(CH_2C_5H_4N)_4(CH_3OH)_4Cl_4$	6	−0.64	−5.6	0	0	uniaxial	[26]	[27]
$Fe_4(OCH_2)_6(C_4H_9ON)_6$	5	−0.56	−0.57	0.06	0.05	triaxial	[28]	[29]
$Cr[N(Si(CH_3)_3)_2]_3$	3/2	−2.49	−2.66	0	0	uniaxial		[30]

The HOMO and the LUMO belong to the majority spin channel and the gap is quite small 0.45 eV [7]. The density of states near the Fermi level is dominated by the Mn 3d states and also has some contribution from oxygen 2p states. Although the states near the Fermi level belong to the majority spin channel, it is actually the majority occupied and minority unoccupied states which contribute nearly 65% of the anisotropy barrier.

3.2. Mn_{10} cluster

The $[Mn_{10}O_4(2,2'\text{-biphenoxide})_4Br_{12}]^{4-}$ functional unit is compensated by $[CH_3CH_2)_3NH]_2[Mn(CH_3CN)_4(H_2O)_2]$. Experimental results suggest that the magnetic anisotropy is due to the localized valence electrons of the ten Mn atoms and our calculations on the $[CH_3CH_2)_3NH]_2[Mn(CH_3CN)_4(H_2O)_2]$ confirm that this unit behaves as a charge compensating paramagnetic spectator. High-field EPR measurements have determined that the molecule in its ground state has spin $S = 12$. However, our calculations have shown that this spin state would not be magnetically stable since there would be no common Fermi level in the majority and minority channels. As a result we obtained a $S = 13$ spin state. This is consistent with experiment since it is difficult to differentiate between the two possibilities experimentally [31].

The majority gap in Mn_{10} is also much smaller than the minority one [24]. In Mn_{10}, all matrix elements from the occupied majority electrons prefer an easy-axis system whereas the matrix elements from the occupied minority spin channel would result in an easy-plane system. There is a competition between these possibilities and due to the larger contribution from the occupied majority spin channel the system ends up as an easy-axis system. Therefore, in spite of the fact that Mn_{10} possesses a high-spin state, the anisotropy barrier in this system is small. The calculated barrier height of 9.5 K compares reasonably well with the experimental value of 7.7 K [25]. We found that the removal of subsets of the Br ions will change the magnetic anisotropy drastically by changing the electronic structure. However, neutralizing the electric field due to Br ions by an external potential in the calculations changed the anisotropy barrier by less than 1 K. Therefore, we conclude that the electric fields created by the Br ions do not have a significant effect on the magnetic properties of the molecule in contrast to chemical interactions.

3.3. Fe_4-star

While the molecular structure of the other examples is well known or has been discussed in detail in an earlier publication it seems to be worthwhile to give the structure for this case to demonstrate the magnetic ordering. In the Ferric star or the Fe_4 cluster shown in Fig. 1, all iron atoms are Fe^{3+}-ions, the inner Fe is coupled antiferromagnetically to the outer Fe atoms, resulting in a ferrimagnetic spin-ordering with total $S = 5$. The calculated values in Table 2 for the Fe_4 are preliminary, and therefore, we postpone a detailed discussion of that system to a forthcoming publication.

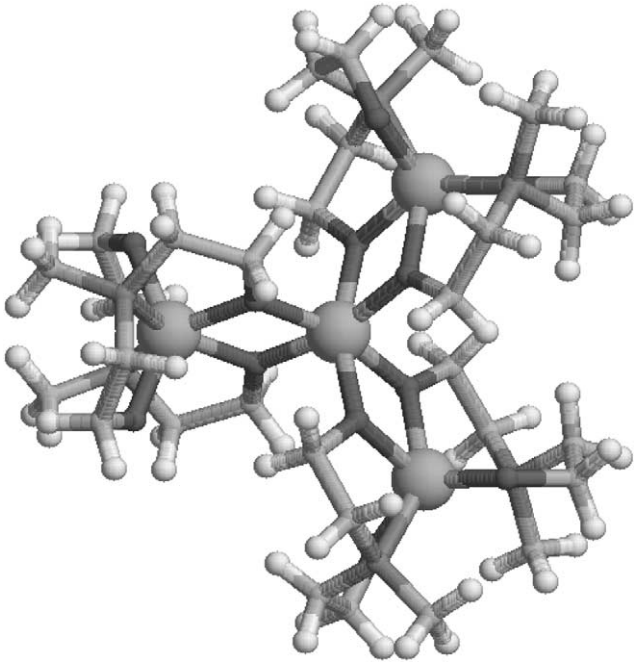

Fig. 1. The molecular structure of the Fe_4-star. The four Fe atoms are shown by large spheres.

3.4. Co_4 cluster

Co_4 displays ferromagnetic ordering. In the case of Co_4, the experimental determination of the D parameter is not conclusive. Our calculations showed that in this system the anisotropy barrier has a large pressure gradient [26]. During the optimization cycle, the distance between the hydroxymethyl pyridine ligands were found to increase, which in turn led to an increase of the HOMO–LUMO gap and consequent reduction of the anisotropy barrier. The barrier during the optimization was found to vary between 60 and 23 K. In the crystalline environment, the ligands are likely to be pressed towards each other and that may lead to a high value of barrier. Since, the calculations are performed on isolated systems where such effects are absent, the barrier is also lower than the experimentally determined value. On the other hand our calculations showed that when the geometry of the molecule is changed from the lowest-energy staggered geometry to a higher energy eclipsed geometry, the system has triaxial anisotropy and the anisotropy barrier increases to 95 K. Another high-energy isomer which lies between the staggered and the eclipsed structure, has an easy-plane anisotropy with a barrier of 50 K. Therefore, any experiment which can change the orientation of the ligands, can achieve higher barrier.

3.5. Cr-amide

The Cr-amide $Cr[N(Si(CH_3)_3)_2]_3$ contains only a single magnetic center (Cr^{3+}) located in the middle of the molecule threefold coordinated by nitrogen atoms (see Fig. 2). The charge state is confirmed by calculating the spin density within a sphere around the Cr atom. A sphere with radius of 1.2 Å contains already 2.7 majority

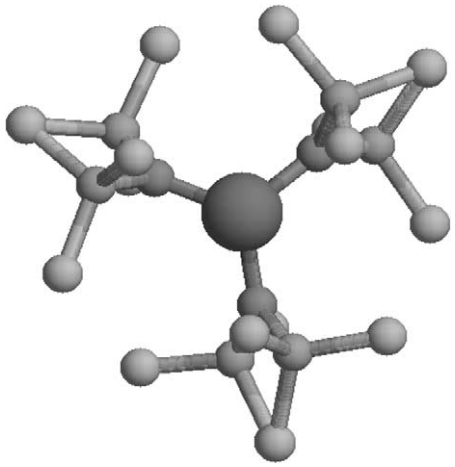

Fig. 2. The molecular structure of the Cr-amide. The Cr atom in the center is shown by the large sphere. Hydrogens are not displayed for clarity.

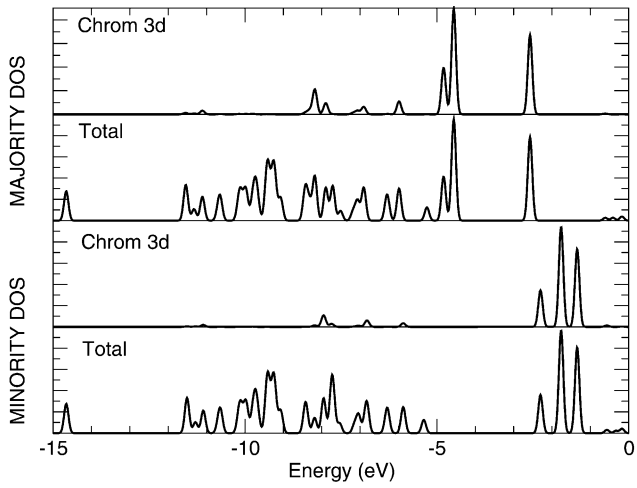

Fig. 3. The electronic density of states of the Cr-amide. The HOMO is derived from Cr majority 3d spin states at −5 eV. The molecular levels have been broadened by a Gaussian.

electron, clearly confirming the Cr^{3+} charge state. The electronic density of states obtained from Gaussian broadened molecular levels is presented in Fig. 3. The HOMO comes from Cr majority 3d states at around −5 eV. The Cr_1 molecule has large majority and minority gaps on the order of 2 to 2.5 eV, respectively. The anisotropy barrier in this molecule is small (Table 2) which can be attributed to the large HOMO–LUMO gap. In this case, the spin density is well localized on the Cr atom. The HOMO and LUMO states are definitely Cr(3d) and there is some covalent bonding between the Cr states and the ligands. The magnetic behavior is completely determined by the Cr states. This is an interesting case. Since the spin is small (3/2) there is only one magnetic field at which resonant tunneling of magnetization would be achieved. However, no such experimental measurements have been reported so far. The calculated magnetic anisotropy barrier of 5.6 K agrees well with the experimental value of 6 K obtained from electron spin resonance measurements [30].

3.6. V_{15} spin system

Finally we mention that the anisotropy energy in the V_{15} spin system has also been approximately determined using the same method discussed above. In contrast to the other molecules mentioned herein the V_{15} has an anisotropy energy that nearly vanishes and the interesting physics in this system is due to a large number of nearly degenerate spin configurations which are energetically differentiated by exchange interactions and only weakly affected by anisotropies. While direct measurements of the anisotropy energy in this system are presently unavailable, we point out that the observed field-induced crossing between the (3/2, 1/2) states and

(1/2, 1/2) state is reasonably in accord with the small anisotropy calculated in this system. See Ref. [32] for details.

4. Summary

It is observed that although a small value of the energy differences between the occupied and unoccupied states would result in a high value of the anisotropy barrier, it is also necessary for the states to have substantial overlap. Also, it is extremely important to obtain the correct charge states for the calculation of the barrier [33,34]. An incorrect charge transfer can drastically affect the accuracy of the results.

In conclusion, we reviewed a method for the calculation of the magnetic anisotropy barrier from single particle wavefunctions. The spin–orbit operator was expanded in an exact Cartesian formulation and we show that it leads to accurate predictions of the anisotropy barrier in a number of cases. We also discuss the importance of using the correct geometry, spin-ordering and charge states in the calculation.

In order to explore the range of systems where the presented method gives reliable results, further studies on more systems are needed. Also the study of experimentally well characterized classes of compounds where only the ligands are changed in a controlled way but not the magnetic core would show if our calculational approach can reproduce the observed changes in the magnetic behavior. Our current results make us very confident in the predictive power of the presented method. This should allow for a microscopic understanding based on the electronic structure of single molecule magnets of the magnetic anisotropy parameters which is crucial for a design of molecular nanomagnets. In particular the results suggest that there is sufficient accuracy for the computationally aided design of technologies based on these systems.

Acknowledgements

J.K. would like to thank the Schloeßmann Foundation for financial support. T.B. and M.R.P. gratefully acknowledge the financial support by ONR grant N0001400WX2011. M.R.P., C.S.H. and N.B. acknowledge partial support for CHSSI and NRL. We would like to thank R. Sessoli for many stimulating discussions and S. Schromm, O. Wald-mann, P. Müller for communicating to us their unpublished results on the Fe_4-star.

References

[1] R. Sessoli, D. Gatteschi, A. Caneschi, M.A. Novak, Nature (London) 365 (1993) 141.
[2] (a) J. Friedman, M.P. Sarachik, J. Tejeda, J. Maciejewski, R. Ziolo, Phys. Rev. Lett. 76 (1996) 3820;
(b) L. Thomas, F. Lionti, R. Ballou, D. Gatteschi, R. Sessoli, B. Barbara, Nature (London) 383 (1996) 145.
[3] W. Wernsdorfer, R. Sessoli, Science 284 (1999) 133.
[4] M.N. Leuenberger, D. Loss, Nature 410 (2001) 789.
[5] J. Van Vleck, Phys. Rev. 52 (1937) 1178.
[6] J.S. Miller, Polyhedron 20 (2001) 1723.
[7] M.R. Pederson, S.N. Khanna, Phys. Rev. B 60 (1999) 9566.
[8] http://www.physics.nist.gov/PhysRefData/DFTdata/contents.html.
[9] M.R. Pederson, A.Y. Liu, T. Baruah, E.Z. Kurmaev, A. Moewes, S. Chiuzbaian, M. Neumann, C.R. Kmety, K.L. Stevenson, D. Ederer, Phys. Rev. B 66 (2002) 014446.
[10] Y. Hirai, I. Zivkovic, B.H. Frazer, A. Reginelli, L. Perfetti, D. Ariosa, G. Margaritondo, M. Prester, D. Drobac, D.T. Jiang, Y. Hu, T.K. Sham, I. Felner, M. Pederson, M. Onellion, Phys. Rev. B 65 (2002) 054417.
[11] P. Hohenberg, W. Kohn, Phys. Rev. 136 (1964) B864.
[12] W. Kohn, L.J. Sham, Phys. Rev. 140 (1965) A1133.
[13] M.R. Pederson, K.A. Jackson, Phys. Rev. B 41 (1990) 7453.
[14] K.A. Jackson, M.R. Pederson, Phys. Rev. B 42 (1990) 3276.
[15] A. Briley, M.R. Pederson, K.A. Jackson, D.C. Patton, D.V. Porezag, Phys. Rev. A 58 (1998) 1786.
[16] D.V. Porezag, M.R. Pederson, Phys. Rev. B 54 (1996) 7830.
[17] D.V. Porezag, M.R. Pederson, Phys. Rev. A 60 (1999) 9566.
[18] M.R. Pederson, D.V. Porezag, J. Kortus, D.C. Patton, Phys. Stat. Solidi (b) 217 (2000) 197.
[19] J.P. Perdew, K. Burke, M. Ernzerhof, Phys. Rev. Lett. 77 (1996) 3865.
[20] (a) H. Hellmann, Einführung in die Quantentheorie, Deuticke, Leipzig, 1937;
(b) R.P. Feynman, Phys. Rev. 56 (1939) 340;
(c) P. Pulay, Mol. Phys. 17 (1969) 197.
[21] http://cst-www.nrl.navy.mil/ ~ nrlmol.
[22] M.R. Pederson, S.N. Khanna, Chem. Phys. Lett. 307 (1999) 253.
[23] K.M. Mertes, Y. Suzuki, M.P. Sarachik, Y. Paltiel, H. Shtrikman, E. Zeldov, E. Rumberger, D.N. Hendrickson, G. Christou, Phys. Rev. Lett. 87 (2001) 227205.
[24] J. Kortus, T. Baruah, N. Bernstein, M.R. Pederson, Phys. Rev. B 66 (2002) 092403.
[25] A.L. Barra, A. Caneschi, D. Gatteschi, D.P. Goldberg, R. Sessoli, J. Solid State Chem. 145 (1999) 484.
[26] T. Baruah, M.R. Pederson, Chem. Phys. Lett. 360 (2002) 144.
[27] E.C. Yang, D.N. Hendrickson, W. Wernsdorfer, M. Nakano, R. Sommer, A.L. Rheingold, M. Ledezma-Gairaud, cond-mat/0109219.
[28] J. Kortus, M.R. Pederson, in press.
[29] S. Schromm, O. Waldmann, P. Müller, University of Erlangen, private communication.
[30] D.C. Bradley, R.G. Copperthwaite, S.A. Cotton, K.D. Sales, J.F. Gibson, J. Chem. Soc., Dalton Trans. 2 (1973) 191.
[31] R. Sessoli, private communication.
[32] J. Kortus, C.S. Hellberg, M.R. Pederson, Phys. Rev. Lett. 86 (2001) 3400.
[33] J. Kortus, M.R. Pederson, C.S. Hellberg, S.N. Khanna, Eur. Phys. J. D 16 (2001) 177.
[34] M.R. Pederson, J. Kortus, S.N. Khanna, J. Appl. Phys. 91 (2002) 7149.